

# Keeping the Universe ionised: Photo-ionisation heating and the critical star formation rate at redshift $z \approx 6$

Andreas H. Pawlik<sup>1\*</sup>, Joop Schaye<sup>1†</sup> and Eveline van Scherpenzeel<sup>1</sup>

<sup>1</sup>*Leiden Observatory, Leiden University, P.O. Box 9513, 2300RA Leiden, The Netherlands*

Accepted; Received; in original form

## ABSTRACT

The critical star formation rate density required to keep the intergalactic hydrogen ionised depends crucially on the average rate of recombinations in the intergalactic medium (IGM). This rate is proportional to the clumping factor  $C \equiv \langle \rho_b^2 \rangle_{\text{IGM}} / \langle \rho_b \rangle^2$ , where  $\rho_b$  and  $\langle \rho_b \rangle$  are the local and cosmic mean baryon density, respectively and the brackets  $\langle \rangle_{\text{IGM}}$  indicate spatial averaging over the recombing gas in the IGM. We perform a suite of cosmological smoothed particle hydrodynamics simulations that include radiative cooling to calculate the volume-weighted clumping factor of the IGM at redshifts  $z \geq 6$ . We focus on the effect of photo-ionisation heating by a uniform ultraviolet background and find that photo-heating strongly reduces the clumping factor because the increased pressure support smoothes out small-scale density fluctuations. Photo-ionisation heating is often said to provide a negative feedback on the reionisation of the IGM because it suppresses the cosmic star formation rate by boiling the gas out of low-mass halos. However, because of the reduction of the clumping factor it also makes it easier to keep the IGM ionised. Photo-heating therefore also provides a positive feedback which, while known to exist, has received much less attention. We demonstrate that this positive feedback is in fact very strong. Using conservative assumptions, we find that if the IGM was reheated at  $z \gtrsim 9$ , the observed population of star-forming galaxies at  $z \approx 6$  may be sufficient to keep the IGM ionised, provided that the fraction of ionising photons that escape the star-forming regions to ionise the IGM is larger than 0.2.

**Key words:** cosmology: theory - methods: numerical - hydrodynamics - radiative transfer - intergalactic medium - galaxies: formation

## 1 INTRODUCTION

The absence of a Gunn-Peterson trough in the majority of the observed line-of-sight spectra towards high-redshift quasars suggests that the reionisation of intergalactic hydrogen was completed at a redshift  $z \gtrsim 6$  (see Fan, Carilli, & Keating 2006 for a recent review) and that it remained highly ionised ever since. Current observational estimates of the ultraviolet (UV) luminosity density at redshifts  $z \lesssim 6$  (e.g. Stanway, Bunker, & McMahon 2003; Bunker et al. 2004; Bouwens et al. 2004; Sawicki & Thompson 2006; Bouwens et al. 2006; Mannucci et al. 2007; Oesch et al. 2008; Bouwens et al. 2008), on the other hand, may imply star formation rate (SFR) densities several times lower than the critical SFR density required to keep the intergalactic medium (IGM) ionised. Taken at face value, these low SFR

densities pose a severe challenge to commonly employed theoretical models in which the observed population of star-forming galaxies is the only source of ionising radiation in the high-redshift Universe.

There are, however, large uncertainties associated with both the observed (see, e.g., the comprehensive analysis of Bouwens et al. 2007) and the critical SFR densities. The critical SFR density,

$$\dot{\rho}_* \approx 0.027 \text{ M}_\odot \text{ yr}^{-1} \text{ Mpc}^{-3} \times f_{\text{esc}}^{-1} \left( \frac{C}{30} \right) \left( \frac{1+z}{7} \right)^3 \left( \frac{\Omega_b h^2_{70}}{0.0465} \right)^2, \quad (1)$$

here rescaled to match the most recent WMAP estimate for the cosmic baryon density (Komatsu et al. 2008), has been derived by Madau, Haardt, & Rees (1999) using an early version of the Bruzual & Charlot (2003) population synthesis code, assuming a Salpeter initial stellar mass function (IMF) and solar metallicity. It is inversely proportional to the escape fraction  $f_{\text{esc}}$ , i.e. the fraction of ionising photons produced by star-forming galaxies that escape the in-

\* E-mail: pawlik@strw.leidenuniv.nl

† E-mail: schaye@strw.leidenuniv.nl

terstellar medium (ISM) to ionise the IGM, and proportional to the recombination rate in the IGM. The latter is often parametrised using the dimensionless clumping factor  $C \equiv \langle \rho_b^2 \rangle_{\text{IGM}} / \langle \rho_b \rangle^2$ , where  $\rho_b$  is the baryon density,  $\langle \rho_b \rangle$  is the mean baryon density of the Universe and the brackets  $\langle \rangle_{\text{IGM}}$  indicate spatial averaging over the gas constituting the recombining IGM. Under the assumption of a uniformly ionised IGM, the clumping factor expresses the spatially averaged number of recombinations occurring per unit time and unit volume in the ionised IGM, relative to that in gas at the cosmic mean density  $\langle \rho_b \rangle$ . A larger escape fraction implies a smaller critical SFR density, as more photons are available to ionise the IGM. On the other hand, a larger clumping factor implies a larger critical SFR density since more ionising photons are required to compensate for the increased number of recombinations.

Most observational studies that compare<sup>1</sup> the SFR density derived from estimates of the UV luminosity density at redshift  $z \approx 6$  to the critical SFR density assume an escape fraction  $f_{\text{esc}} \lesssim 0.5$  and a clumping factor  $C = 30$ . While a variety of both observational and theoretical studies (e.g. Inoue, Iwata, & Deharveng 2006 and references therein; Razoumov & Sommer-Larsen 2006; Gnedin, Kravtsov, & Chen 2008) have ruled out larger escape fractions, the estimate for the clumping factor comes from a single cosmological simulation performed more than 10 years ago (Gnedin & Ostriker 1997). It is on the basis of these values for the escape fraction and the clumping factor that the observed population of galaxies has been found to be incapable of keeping the intergalactic hydrogen ionised, forming massive stars at a rate which is up to an order of magnitude lower than required by Eq. 1.

It has been pointed out that this discrepancy between the inferred and critical SFR densities could be resolved if the employed clumping factor were too high (e.g. Stiavelli, Fall, & Panagia 2004; Sawicki & Thompson 2006; see also the discussion in Bouwens et al. 2007). Indeed, in most (but not all) of the more recent theoretical studies (e.g. Valageas & Silk 1999; Miralda-Escudé, Haehnelt, & Rees 2000; Gnedin 2000a; Haiman, Abel, & Madau 2001; Benson et al. 2001; Chiu, Fan, & Ostriker 2003; Iliev et al. 2007; Srbnovsky & Wyithe 2007; Kohler, Gnedin, & Hamilton 2007; Bolton & Haehnelt 2007; Maio et al. 2007; Furlanetto, Haiman, & Oh 2008) significantly lower clumping factors were derived. On the other hand, it is sometimes emphasised that simulations underestimate the clumping factor, due to a lack of resolution (see, e.g., Madau, Haardt, & Rees 1999). In this work we perform a set of cosmological Smoothed Particle Hydrodynamics (SPH) simulations that include radiative cooling and photo-ionisation by a uniform UV background in the optically thin limit to study the clumping factor of the IGM.

We focus on the effect of photo-ionisation heating on the evolution of the clumping factor. Previous investigations of the impact of photo-heating on the reionisation of the IGM have almost exclusively come to the conclu-

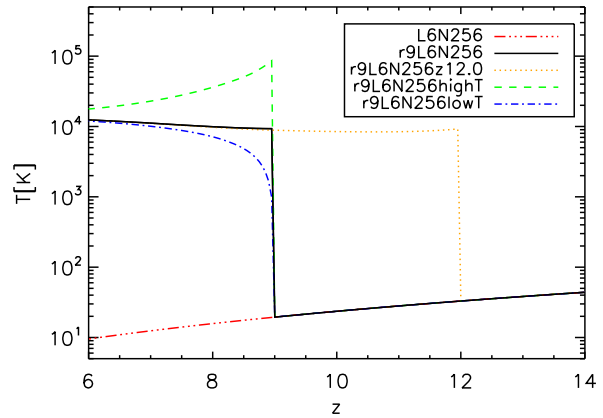


**Figure 1.** Thermal evolution of gas with overdensity  $\Delta = 1$  for characteristic choices of the reheating parameters  $z_r$  and  $\epsilon_r$ , which are listed in Table 1 for the simulations indicated in the legend. Note that even in the absence of an additional energy input at redshift  $z = z_r$ , i.e. for  $\epsilon_r = 0$ , as it is the case for simulation *r9L6N256lowT*, the gas is quickly heated by the UV background to a temperature  $T \sim 10^4$  K.

sion that it acts as to provide a negative feedback. Photo-heating boils the gas out of the potential wells of dark matter (DM) halos with virial temperatures  $T_{\text{vir}} \lesssim 10^4$  K (e.g. Thoul & Weinberg 1996; Navarro & Steinmetz 1997; Barkana & Loeb 1999; Kitayama & Ikeuchi 2000; Gnedin 2000b; Dijkstra et al. 2004; Shapiro, Iliev, & Raga 2004; Mesinger & Dijkstra 2008; Okamoto, Gao, & Theuns 2008), inhibiting the formation of stars in these low-mass halos and thus decreasing the ionising emissivity. The same mechanism that reduces the number of ionising photons that are emitted into the IGM does, however, also affect the evolution of the clumping factor (e.g. Haiman, Abel, & Madau 2001; Oh & Haiman 2003; Kuhlen & Madau 2005; Wise & Abel 2005; Ciardi & Salvaterra 2007). In this paper we demonstrate that photo-heating significantly lowers the clumping factor and hence the average recombination rate in the IGM. While photo-ionisation heating undoubtedly impedes the production of ionising photons, our results imply that it also makes it much easier to keep the IGM ionised.

This paper is structured as follows. In Section 2 we give a detailed description of our set of simulations. In Section 3 we use our simulations to compute the clumping factor of the IGM. Finally, in Section 4, we discuss our results and their implications for the value of the critical SFR density.

## 2 SIMULATIONS

We use a modified version of the N-body/TreePM/SPH code GADGET-2 (Springel 2005) to perform a suite of cosmological SPH simulations including radiative cooling.

The initial particle positions and velocities are obtained from glass-like initial conditions using CMBFAST (version 4.1; Seljak & Zaldarriaga 1996) and employing the Zeldovich approximation to linearly evolve the particles down to redshift  $z = 127$ . We assume a flat  $\Lambda$ CDM universe and employ the set of cosmological parameters  $[\Omega_m, \Omega_b, \Omega_\Lambda, \sigma_8, n_s, h]$

<sup>1</sup> Note that this comparison is insensitive to the IMF provided the same IMF is used to compute the critical and observationally derived SFR densities.

**Table 1.** Simulation parameters: comoving size of the simulation box,  $L_{\text{box}}$  (default value:  $6.25 h^{-1}$  Mpc); number of DM particles,  $N_{\text{dm}}$  (default value:  $256^3$ ); mass of dark matter particles,  $m_{\text{dm}}$  (default value:  $8.6 \times 10^5 h^{-1} M_{\odot}$ ); additional reheating energy per proton,  $\epsilon_r$  (default value: 2 eV); reheating redshift,  $z_r$  (default value: 9); kinetic feedback from supernova winds, winds (default: no); cosmological parameters, WMAP (default: 5-year). The number of SPH particles initially equals  $N_{\text{dm}}$  (it decreases during the simulation due to star formation).

Simulation	$L_{\text{box}}$ [ $h^{-1}$ comoving Mpc]	$N_{\text{dm}}$	$m_{\text{dm}}$ [ $10^5 h^{-1} M_{\odot}$ ]	$\epsilon_r$ [ eV]	$z_r$	winds	WMAP year
<i>r9L6N256</i>	6.25	$256^3$	8.6	2	9	no	5
<i>L6N256</i>	6.25	$256^3$	8.6	0	0	no	5
<i>r[<math>z_r</math>]L6N256</i>	6.25	$256^3$	8.6	2	[7.5, 10.5, 12, 13.5, 15, 19.5]	no	5
<i>r9L6N256highT</i>	6.25	$256^3$	8.6	20	9	no	5
<i>r9L6N256lowT</i>	6.25	$256^3$	8.6	0	9	no	5
<i>r9L6N256winds</i>	6.25	$256^3$	8.6	2	9	yes	5
<i>r9L6N256W1</i>	6.25	$256^3$	8.3	2	9	no	1
<i>r9L6N256W3</i>	6.25	$256^3$	7.9	2	9	no	3
<i>r9L12N256</i>	12.5	$256^3$	69.1	2	9	no	5
<i>r9L6N128</i>	6.25	$128^3$	69.1	2	9	no	5
<i>r9L6N064</i>	6.25	$64^3$	552.8	2	9	no	5
<i>r9L3N064</i>	3.125	$64^3$	69.1	2	9	no	5

given by [0.258, 0.0441, 0.742, 0.796, 0.963, 0.719], in agreement with the WMAP 5-year observations (Komatsu et al. 2008). For comparison, we also perform some simulations employing the set of cosmological parameters [0.238, 0.0418, 0.762, 0.74, 0.951, 0.73] and [0.25, 0.045, 0.75, 0.9, 1, 0.73], consistent with WMAP 3-year (Spergel et al. 2007) and WMAP 1-year (Spergel et al. 2003) observations, respectively. Data is generated at 50 equally spaced redshifts between  $z = 20$  and  $z = 6$ . The parameters of the simulations employed for the present work are summarised in Table 1.

The gravitational forces are softened over a length of  $1/25$  of the mean dark matter inter-particle distance. We employ the star formation recipe of Schaye & Dalla Vecchia (2008), to which we refer the reader for details. Briefly, gas with densities exceeding the critical density for the onset of the thermo-gravitational instability (hydrogen number densities  $n_{\text{H}} = 10^{-2} - 10^{-1} \text{ cm}^{-3}$ ) is expected to be multiphase and star-forming (Schaye 2004). We therefore impose an effective equation of state (EOS) with pressure  $P \propto \rho^{\gamma_{\text{eff}}}$  for densities  $n_{\text{H}} > n_{\text{H}}^*$ , where  $n_{\text{H}}^* \equiv 10^{-1} \text{ cm}^{-3}$ , normalised to  $P/k = 10^3 \text{ cm}^{-3} \text{ K}$  at the critical density  $n_{\text{H}}^*$ . We use  $\gamma_{\text{eff}} = 4/3$  for which both the Jeans mass and the ratio of the Jeans length and the SPH kernel are independent of the density, thus preventing spurious fragmentation due to a lack of numerical resolution. Gas on the effective EOS is allowed to form stars using a rate that reproduces the observed Kennicutt-Schmidt law (Kennicutt 1998), renormalised by a factor<sup>2</sup> of  $1/1.65$  to account for the fact that it assumes a Salpeter IMF whereas we are using a Chabrier IMF.

The gas is of primordial composition, with a hydrogen mass fraction  $X = 0.752$  and a helium mass fraction  $Y = 1 - X$ . Radiative cooling and heating are included as-

suming ionisation equilibrium, using tables<sup>3</sup> generated with the publicly available package CLOUDY (version 05.07 of the code last described by Ferland et al. 1998). The gas is allowed to cool by collisional ionisation and excitation, emission of free-free and recombination radiation and Compton cooling off the cosmic microwave background.

We perform a set of simulations including photo-ionisation by a uniform UV background in the optically thin limit at redshifts below the reheating redshift  $z_r$ . These simulations are denoted with the prefix *r* (see Table 1). To study the effect of reionisation reheating, we compare these simulations to a simulation that does not include photo-ionisation (*L6N256*). Note that the photo-ionisation changes the density of free electrons and the ionic abundances. Both the cooling and heating rates are therefore affected by the inclusion of a UV background (e.g. Efstathiou 1992; Wiersma, Schaye & Smith 2008).

The properties of the UV background depend on the redshift of reheating. If  $z_r \leq 9$ , we employ the evolving UV background from quasars and galaxies tabulated by Haardt & Madau (2001) for  $z \leq z_r$ . If  $z_r > 9$ , we use the  $z = 9$  Haardt & Madau (2001) UV background for all redshifts  $9 < z \leq z_r$ , and employ the evolving Haardt & Madau (2001) UV background for redshifts  $z \leq 9$ . This is necessary because Haardt & Madau (2001) only tabulate up to  $z = 9$ . For  $z > z_r$ , we employ the  $z = 9$  Haardt & Madau (2001) UV background but with its intensity at energies equal to and larger than  $13.6 \text{ eV}$  set to zero. Molecular hydrogen and deuterium and their catalysts are kept photo-dissociated by this soft UV background at all redshifts and therefore never contribute to the cooling rate (e.g. Haiman, Rees, & Loeb 1997 and references therein; Glover 2007; Chuzhoy, Kuhlen, & Shapiro 2007).

The reheating redshift  $z_r$  is a parameter in our simulations. The most recent determination of the Thomson optical depth towards reionisation from the WMAP (5-year

<sup>2</sup> This conversion factor between SFRs has been computed using the Bruzual & Charlot (2003) population synthesis code for model galaxies of age  $> 10^7$  yr forming stars at a constant rate and is insensitive to the assumed metallicity.

<sup>3</sup> For a detailed description of the tables see Wiersma, Schaye & Smith (2008).

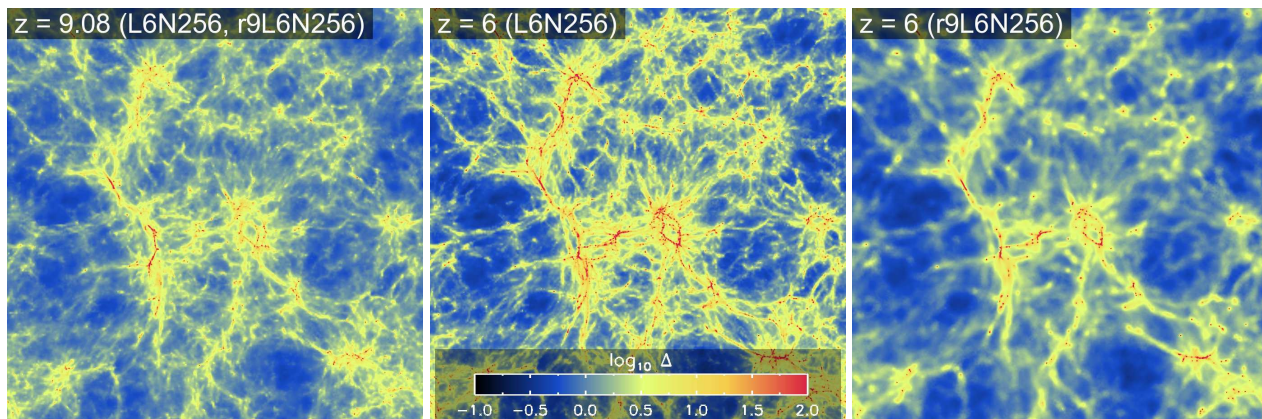


**Figure 2.** Slices (of thickness  $1.25 h^{-1}$  comoving Mpc) through the centre of the simulation box, showing the SPH overdensity field in the simulations *L6N256* and *r9L6N256* at redshifts  $z = 9.08$  (left-hand panel; where they are identical) and  $z = 6$  (middle panel: *L6N256*, right-hand panel: *r9L6N256*). The inclusion of photo-heating in *r9L6N256* leads to a strong smoothing of the density field (right-hand panel).

experiment implies a reionisation redshift  $z_{\text{reion}} = 11.0 \pm 1.4$ , assuming that the transition from the neutral to the fully ionised Universe was instantaneous (Komatsu et al. 2008). The Thomson optical depth towards reionisation provides, however, only an integral constraint on the Epoch of Reionisation. The reionisation history may therefore have been considerably more intricate. An early population of X-ray sources, for example, could reheat the IGM to temperatures  $\sim 10^4$  K already at much higher redshifts (e.g. Collin-Souffrin 1991; Madau & Efstathiou 1999; Oh 2001; Venkatesan, Giroux, & Shull 2001; Machacek, Bryan, & Abel 2003; Madau et al. 2004; Ricotti & Ostriker 2004). We therefore study a range of thermal histories, performing simulations using  $z_r = 7.5, 9, 10.5, 12, 13.5, 15$  and  $19.5$ . To be conservative, we use the relatively low reheating redshift  $z_r = 9$  as our default value.

In our simulations we compute the photo-heating rates in the optically thin limit, which means that we underestimate the temperature of the IGM during reionisation (e.g. Abel & Haehnelt 1999). We therefore inject an additional thermal energy  $\epsilon_r$  per proton at  $z = z_r$  (see, e.g., Thoul & Weinberg 1996). By varying the parameter  $\epsilon_r$ , we will investigate the sensitivity of our results to the temperature of the reheated IGM. Our default simulation employs  $\epsilon_r = 2$  eV. Fig. 1 shows the thermal evolution of gas at the cosmic mean baryon density  $\langle \rho_b \rangle$ , i.e. of gas with overdensity  $\Delta \equiv \rho_b / \langle \rho_b \rangle = 1$ , for different values of  $\epsilon_r$  and  $z_r$ . At  $z = z_r$ , the gas is heated to  $T_r \approx 10^4$  K for  $\epsilon_r = 2$  eV, whereas the gas temperature is about an order of magnitude higher (lower) for  $\epsilon_r = 20$  eV ( $\epsilon_r = 0$  eV). After reheating the gas quickly loses memory of its initial temperature and by  $z = 6$  the gas temperature is  $T \approx 10^4$  K in all cases.

In one of our simulations (*r9L6N256winds*) we include kinetic feedback from star formation. We employ the prescription of Dalla Vecchia & Schaye (2008), which is a variation of the Springel & Hernquist (2003) recipe for kinetic feedback. In this prescription, core-collapse supernovae locally inject kinetic energy and kick gas particles into winds. The feedback is specified by two parameters, the mass loading  $\eta \equiv \dot{M}_w / \dot{M}_*$ , which describes the ini-

tial wind mass loading  $\dot{M}_w$  in units of the cosmic SFR  $\dot{M}_*$ , and the initial wind velocity  $v_w$ . We use  $\eta = 2$  and  $v_w = 600 \text{ km s}^{-1}$ , consistent with observations of local (e.g. Veilleux, Cecil, & Bland-Hawthorn 2005) and redshift  $z \approx 3$  (Shapley et al. 2003) starburst galaxies. Note that wind particles are not hydrodynamically decoupled and that they are launched local to the star formation event, different from the Springel & Hernquist (2003) recipe.

### 3 RESULTS

In this section we employ the set of simulations described in Section 2 and summarised in Table 1 to calculate the clumping factor of the IGM. We start in Section 3.1 with analysing the distribution of the gas in our default simulation *r9L6N256* and in the simulation *L6N256*, which is identical to our default simulation except for the fact that it does not include a photo-ionising background. In Section 3.2 we discuss the definition of the clumping factor and compare the clumping factors derived from our default simulation *r9L6N256* to that derived from simulation *L6N256*. We verify the convergence of our results with respect to variations in the mass resolution and in the size of the simulation box in Section 3.2.1. In Section 3.2.2 we vary the redshift at which the ionising UV background is turned on and in Section 3.2.3 we demonstrate that our conclusions are robust with respect to our choice for the temperature to which the IGM is photo-heated. Finally, in Section 3.2.4 we discuss how kinetic feedback from supernova winds affects our results and quote the clumping factors obtained from the simulations employing WMAP 3-year and 1-year cosmological parameters.

#### 3.1 The gas density distribution

Here we compare the gas distributions in our default simulation *r9L6N256* (in which the UV background is turned on at redshift  $z_r = 9$ ) and in the simulation *L6N256* (which does not include photo-ionisation heating).

Figure 2 shows the overdensities at redshifts  $z = 9.08$

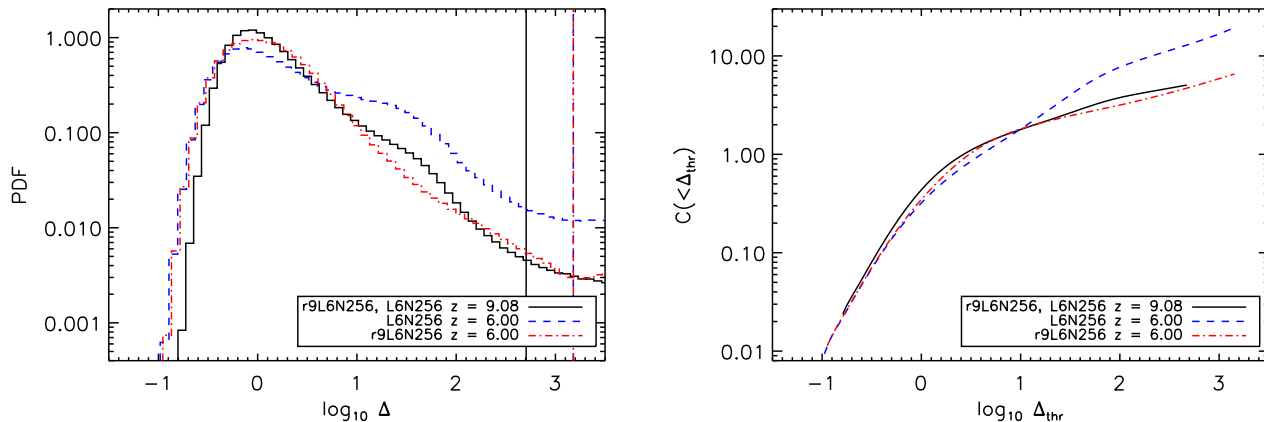


**Figure 3.** *Left-hand panel:* PDF of the baryon overdensity  $\Delta$  per unit  $\log_{10} \Delta$  for simulations  $r9L6N256$  and  $L6N256$  at redshifts  $z = 9.08$  and  $z = 6$ , as indicated in the legend. Photo-heating destroys the bump around overdensities  $1 \lesssim \log_{10} \Delta \lesssim 2$ , which mark the gas that accretes onto DM halos. The vertical lines (which match the colour and style of the corresponding PDFs) indicate the overdensities corresponding to the onset of star formation. *Right-hand panel:* Clumping factor  $C(< \Delta_{\text{thr}})$  of gas with overdensity  $\Delta < \Delta_{\text{thr}}$  for the simulations shown in the left-hand panel. The inclusion of photo-heating in  $r9L6N256$  leads to a clumping factor that is substantially smaller than that obtained from  $L6N256$ , for threshold overdensities  $\Delta_{\text{thr}} > 10$ . Note that the maximum threshold overdensities we consider for the calculation of the clumping factor are given by the critical density  $n_{\text{H}}^* \equiv 10^{-1} \text{ cm}^{-3}$  for the onset of star-formation (the vertical lines shown in the left-hand panel).

and  $z = 6$  in a slice through the simulation box for these simulations. Heating by the photo-ionising background almost instantaneously increases the gas temperatures to  $T_r \sim 10^4$  K (see Fig. 1) and accordingly raises the cosmological Jeans mass. Gas that had already settled into the potential wells of DM halos with virial temperature  $T_{\text{vir}} \lesssim T_r$  is driven back into the diffuse IGM by the increased pressure gradient forces (e.g. Barkana & Loeb 1999; Shapiro, Iliev, & Raga 2004). The large cosmological Jeans mass prevents any re-accretion of gas or infall of previously unbound gaseous material into these low-mass halos and keeps the IGM diffuse. Comparing the middle panel with the right-hand panel of Fig. 2, this *Jeans mass filtering* (e.g. Shapiro, Giroux, & Babul 1994; Gnedin & Hui 1998; Gnedin 2000b; Okamoto, Gao, & Theuns 2008) in the presence of photo-heating leads to a strong smoothing of the small-scale density fluctuations by  $z = 6$ .

A more detailed analysis of the overdensity distribution in the simulations can be obtained by studying  $\mathcal{P}(\Delta)$ , the probability density function (PDF) for  $\Delta$ . In the left-hand panel of Fig. 3 we show  $\mathcal{P}(\Delta)$ , normalised such that  $\int_0^\infty d\Delta \mathcal{P}(\Delta) = 1$ . At redshift  $z = 9.08$  (black solid histogram), the gravitational amplification of the overdensities present in the initial conditions has produced a significant deviation of the PDF from its primordial Gaussian shape. The flattening of the slope of the PDF for overdensities  $1 \lesssim \log_{10} \Delta \lesssim 2$  can be attributed to the shock-heating of gas falling into the potential wells of dark matter halos, most of which have virial temperatures  $\lesssim 10^4$  K, which we refer to as low-mass halos. The shape of the PDF is determined by the effective EOS once the gas reaches the critical density for the onset of star formation ( $n_{\text{H}}^* \equiv 10^{-1} \text{ cm}^{-3}$ , see Section 2; indicated by the vertical lines).

At redshifts  $z < z_r$ , the shape of the PDF strongly depends on whether photo-heating by the ionising background is included or not. In the absence of such a background

( $L6N256$ , blue dashed histogram), gravitational collapse proceeds unimpeded, increasing the PDF at  $\log_{10} \Delta \gtrsim 1$ . Since the gas that accretes onto DM halos must originate from the reservoir at  $\log_{10} \Delta \lesssim 1$  (the diffuse IGM), the PDF decreases over this range of overdensities. As a result, the maximum of the PDF shifts to lower overdensities. At the same time, the gravitational amplification of large-scale underdense regions leads to a slight increase in the PDF around overdensities  $\log_{10} \Delta \sim -1$ . Photo-heating in the presence of the ionising background photo-evaporates the gas in DM halos, as described above. The bump in the PDF around  $1 \lesssim \log_{10} \Delta \lesssim 2$  therefore disappears (red dot-dashed histogram). Note that the redistribution of the baryons due to photo-heating also slightly increases the minimum overdensity that is present in the simulation.

### 3.2 The clumping factor

In this section we demonstrate how the clumping factor,  $C \equiv \langle \rho_b^2 \rangle_{\text{IGM}} / \langle \rho_b \rangle^2$ , depends on the definition of the IGM and compute it for our default simulation  $r9L6N256$  and for the simulation  $L6N256$ . This allows us to investigate how the clumping factor is affected by the inclusion of a photo-ionising background.

Our main motivation for computing the clumping factor of the IGM is to evaluate the critical SFR density required to keep the IGM ionised. The critical SFR density describes the balance between the number of ionising photons escaping into the IGM (parametrised by the escape fraction) and the number of ionising photons that are removed from the IGM due to photo-ionisations of recombining hydrogen ions (parametrised by the clumping factor). When the ratio of escaping photons to recombining ions is larger than unity, the rate at which galaxies form stars exceeds the critical SFR density and is thus sufficient to keep the IGM ionised. It is important to realise that only recom-

binations leading to the removal of ionising photons *which escaped the ISM of the star-forming regions* contribute to the balance that gives rise to the definition of the critical SFR density. To separate the gas in the ISM from the gas in the IGM, a simple threshold density criterion is often employed (e.g. Miralda-Escudé, Haehnelt, & Rees 2000; see also the discussion in Miralda-Escudé 2003). Ionising photons are counted as escaped once they enter regions with gas densities  $\rho_b < \rho_{\text{thr}}$ . Consequently, only gas with densities  $\rho_b < \rho_{\text{thr}}$ , or equivalently, gas with overdensities  $\Delta < \Delta_{\text{thr}} \equiv \rho_{\text{thr}} / \langle \rho_b \rangle$  should be considered in the evaluation of the clumping factor.

The threshold density  $\rho_{\text{thr}}$  depends on which gas is considered to be part of the ISM, and which gas is considered to be part of the IGM. As long as the definition of the escape fraction and that of the clumping factor refer to the same decomposition of the gas into IGM and ISM, its value can be chosen arbitrarily. We therefore treat the threshold density as a parameter and compute the clumping factor as a function of  $\Delta_{\text{thr}}$  (cp. Miralda-Escudé, Haehnelt, & Rees 2000),

$$C(< \Delta_{\text{thr}}) \equiv \int_0^{\Delta_{\text{thr}}} d\Delta \Delta^2 \mathcal{P}(\Delta), \quad (2)$$

where  $\mathcal{P}(\Delta)$  is normalised according to  $\int_0^{\Delta_{\text{thr}}} d\Delta \mathcal{P}(\Delta) = 1$ . In practice, we calculate  $C(< \Delta_{\text{thr}})$  by performing a volume-weighted summation over all SPH particles with overdensities  $\Delta_i < \Delta_{\text{thr}}$ , i.e

$$C(< \Delta_{\text{thr}}) = \frac{\sum_{\Delta_i < \Delta_{\text{thr}}} h_i^3 \Delta_i^2}{\sum_{\Delta_i < \Delta_{\text{thr}}} h_i^3}, \quad (3)$$

where  $h_i$  is the radius of the SPH smoothing kernel associated with SPH particle  $i$ . We verified that replacing  $h_i^3$  with  $m_i/\rho_i$  as an estimate for the volume occupied by SPH particle  $i$  (with mass  $m_i$ ) gives nearly indistinguishable results.

By definition,  $C(< \Delta_{\text{thr}})$  increases monotonically with the threshold density  $\rho_{\text{thr}}$ . Here, we set an upper limit to  $\Delta_{\text{thr}}$ , corresponding to the threshold density  $n_{\text{H}}^* \equiv 10^{-1} \text{ cm}^{-3}$  for the onset of star formation that we employ in our simulations. Since we impose an effective EOS for gas with densities larger than  $n_{\text{H}}^*$  (Section 2), its PDF is not expected to reflect the PDF of real star-forming regions, motivating our choice for the maximum threshold density. The choice is conservative, leading to an overestimate rather than an underestimate of the critical SFR density, since the threshold density marking the escape of ionising photons and hence the clumping factor of the IGM to be used in Eq. 1 is likely to be lower.

In the right-hand panel of Fig. 3 we show  $C(< \Delta_{\text{thr}})$  for the simulations *r9L6N256* and *L6N256* at redshifts shortly before (at  $z = 9.08$ , when *r9L6N256* and *L6N256* are identical) and well after (at  $z = 6$ , when they differ by the presence and absence of an ionising background, respectively) the reheating redshift  $z_r = 9$ . In agreement with our discussion above, the clumping factor increases monotonically with the threshold density. Its dependence on redshift can be understood by looking at the evolution of the shape of the PDF, which we discussed in the previous section.

For *L6N256*, i.e. in the absence of photo-heating, the clumping factor for threshold overdensities  $\log_{10} \Delta_{\text{thr}} > 1$  is larger at  $z = 6$  than at  $z = 9.08$ , due mainly to the

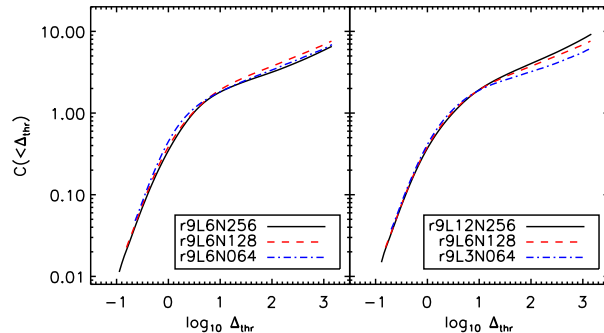


**Figure 4.** Clumping factor  $C(< \Delta_{\text{thr}})$  of gas with overdensities  $\Delta < \Delta_{\text{thr}}$  and its dependence on resolution (at fixed box size, left-hand panel) and on box size (at fixed resolution, right-hand panel). The clumping factor obtained from our default simulation *r9L6N256* is converged.

growth of the bump present in the PDF for overdensities  $1 \lesssim \log_{10} \Delta \lesssim 2$ . For  $\log_{10} \Delta_{\text{thr}} \sim 0$ , on the other hand, the clumping factor is slightly smaller at  $z = 6$  than at  $z = 9.08$ , which is caused by the depletion of the diffuse IGM through accretion onto DM halos. Note that at  $z = 6$  the clumping factor reaches a maximum value of  $C \approx 20$ , which is significantly smaller than the value quoted by Gnedin & Ostriker (1997), which is commonly employed in observational studies. This is probably because Gnedin & Ostriker (1997) computed the clumping factor including gas of any density, i.e. using a density threshold  $\Delta_{\text{thr}} = \infty$  (but see our remarks on convergence in the next section).

The evolution of the clumping factor in *r9L6N256*, i.e. in the presence of the ionising background, is very different. At  $z = 6$  it is close to that at  $z = 9.08$  for all threshold overdensities. Compared to *L6N256*, the difference between the clumping factors for  $z = 6$  and  $z = 9.08$  is greatly reduced and the clumping factor at redshift  $z = 6$  never reaches values larger than  $C \approx 6$ .

### 3.2.1 Convergence tests

In this section we check whether our results are converged. Generally, one expects the clumping factor to increase with both the spatial resolution and the size of the simulation box. The spatial resolution determines the smallest scale on which fluctuations in the density field may be identified, whereas the size of the simulation box sets a cut-off to the largest scale on which the overdensity field can be non-zero. Moreover, the size of the simulation box limits the mass of the largest halo present in the simulation. Fig. 4 demonstrates that our default simulation (*r9L6N256*) is of sufficiently high resolution and employs a sufficiently large box to allow a faithful computation of the clumping factor of the reheated IGM at  $z = 6$ . In the left-hand panel we show the clumping factor in three simulations that use the same box size, but have mass resolutions that differ by multiples of  $2^3$ , whereas in the right-hand panel we show the clumping factor in three simulations that employ the same resolution, but have box sizes that differ by multiples of 2.

When compared to our default simulation *r9L6N256*, decreasing the mass resolution by factors of 8 (*r9L6N128*) and 64 (*r9L6N064*) only leads to insignificant and unsys-

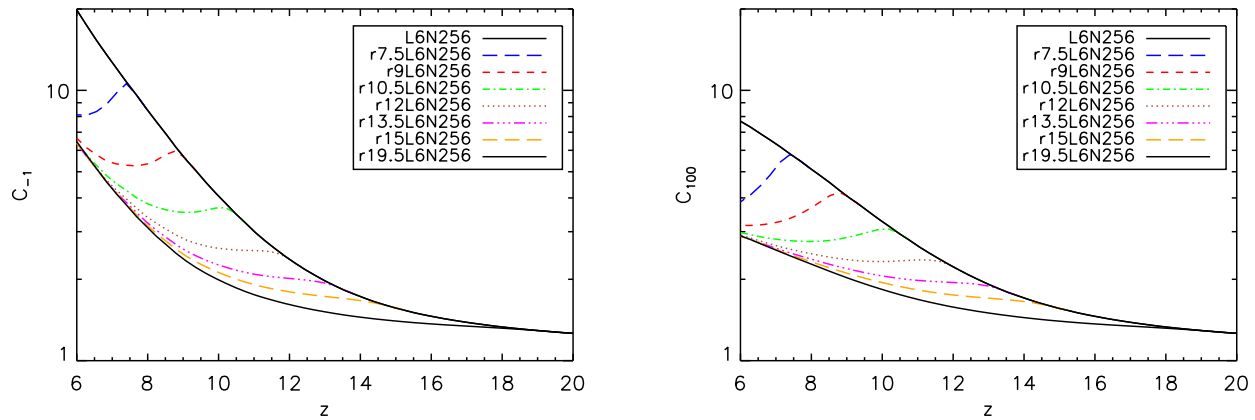


**Figure 5.** Evolution of the clumping factors  $C_{-1}$  (left-hand panel) and  $C_{100}$  (right-hand panel) for different reheating redshifts  $z_r$ , as indicated in the legends. Note that  $C_{-1}(z)$  and  $C_{100}(z)$  in all reheating simulations evolve towards the clumping factors obtained in the simulation with reheating at  $z_r = 19.5$  (bottom black solid curves). At  $z = 6$ , the clumping factors are therefore insensitive to the reheating redshift provided that  $z_r \gtrsim 9$ , with  $C_{-1}(z = 6) \approx 6$  and  $C_{100}(z = 6) \approx 3$ . Fits to the evolution of the clumping factors are given in Appendix A.

tematic<sup>4</sup> changes in the clumping factor (left-hand panel). This can be understood by noting that the virial mass of halos corresponding to a virial temperature  $T_{\text{vir}} = T_r$  is resolved with  $\gtrsim 100$  particles for redshifts  $z < 9$ . Any further increase in resolution would therefore mostly affect the abundance of DM halos with  $T_{\text{vir}} \ll T_r$ . In the presence of the UV background the gas in these halos is, however, quickly photo-evaporated (if formed at  $z > z_r$ ) or prevented from accreting by the large Jeans mass associated with the photo-heated gas (for  $z < z_r$ ). At redshifts well below the reheating redshift  $z_r$ , i.e. when sufficient time has passed to accomplish the photo-evaporation of halos and to allow the gas to respond hydrodynamically to the jump in the Jeans mass (i.e. to Jeans-filter the IGM), the observed convergence with respect to mass resolution is therefore expected<sup>5</sup>.

Since the clumping factor has already converged for the spatial resolution used in simulation *r9L6N128*, we can employ this simulation to verify whether the size of the box of our default simulation *r9L6N256* is sufficiently large to enable an unbiased estimate of the clumping factor (right-hand panel). Clearly, increasing the box size (at fixed resolution) from  $6.25 h^{-1}$  comoving Mpc by a factor of two to  $12.5 h^{-1}$  comoving Mpc leaves the clumping factor almost unaffected. We conclude that our default simulation *r9L6N256* can be safely used to infer the clumping factor of the reheated IGM at  $z = 6$ .

<sup>4</sup> Note that the clumping factor is even slightly larger in *r9L6N128* than in *r9L6N256*, although the latter has an 8 times higher mass resolution.

<sup>5</sup> We note that in the absence of a photo-ionising background, convergence may be more difficult to achieve, requiring a higher mass resolution than employed here. Convergence will be easier to achieve for lower threshold densities.

### 3.2.2 Varying the reheating redshift

To study the effect of photo-heating on the evolution of the clumping factor in more detail, we make use of the clumping factors

$$C_{-1} \equiv C(< 10^{-1} \text{ cm}^{-3} m_{\text{H}} / (X \langle \rho_{\text{b}} \rangle)) \quad (4)$$

and

$$C_{100} \equiv C(< \min(100, 10^{-1} \text{ cm}^{-3} m_{\text{H}} / (X \langle \rho_{\text{b}} \rangle))). \quad (5)$$

$C_{-1}$  is the clumping factor for gas with densities below  $n_{\text{H}} = n_{\text{H}}^* \equiv 10^{-1} \text{ cm}^{-3}$ , the maximum threshold density we consider. For redshifts  $z < 16.3$ ,  $C_{100}$  fixes the threshold overdensity to a value between the mean overdensity of spherical top-hat DM halos, ( $\approx 18\pi^2$ ; e.g. Padmanabhan 1993) and the overdensity at the virial radius of an isothermal DM halo ( $\approx 60$ ; Lacey & Cole 1994) and closely agrees with the threshold densities commonly employed in the literature to calculate the clumping factor of the IGM. For larger redshifts, the threshold overdensity  $\Delta_{\text{thr}} = 100$  corresponds to a density  $n_{\text{H}} > n_{\text{H}}^* \equiv 10^{-1} \text{ cm}^{-3}$ , which is larger than the critical density for the onset of star formation in our simulations. The definition Eq. 5 ensures that the maximum density that we consider for the computation of  $C_{100}$  is always smaller than  $n_{\text{H}}^*$ . Note that  $C_{-1}$  refers to the clumping factor of gas with densities below a fixed proper density, while  $C_{100}$  refers to the clumping factor of gas with densities below a fixed overdensity for redshifts  $z < 16.3$  and is identical to  $C_{-1}$  for larger redshifts.

The evolution of  $C_{-1}$  and  $C_{100}$  is shown, respectively, in the left-hand and right-hand panels of Fig. 5 for the simulations *r9L6N256* (i.e. reheating at redshift  $z_r = 9$ ) and *L6N256* (i.e. no reheating). In the same figure we also include the evolution of  $C_{-1}$  and  $C_{100}$  obtained from the set of simulations  $r[z_r]L6N256z$ , where  $z_r = 7.5, 10.5, 12, 13.5, 15$  and  $19.5$ . While the simulations are identical for  $z > z_r$ , the ionising background strongly affects the evolution of  $C_{-1}(z)$  and  $C_{100}(z)$  for  $z < z_r$ . Whereas in *L6N256* the clumping factors reach  $C_{-1} \approx 20$  and  $C_{100} \approx 8$  at  $z = 6$ , they

only reach  $C_{-1} \approx 6$  and  $C_{100} \approx 3$  in *r9L6N256*, which are smaller than in *L6N256* by roughly a factor of three. Note that because the clumping factor obtained from simulation *L6N256* may not yet be fully converged with respect to resolution (see footnote 5), we may even have underestimated the magnitude of the decrease in the clumping factor due to photo-heating.

Interestingly, the clumping factor at  $z = 6$  is insensitive to the redshift  $z_r$  at which the UV background is turned on, as long as  $z_r \gtrsim 9$ . This is because, after an initial transitory phase, the evolution of the clumping factor obtained for reheating at redshift  $z_r$  approaches that obtained for reheating at  $z_r = 19.5$ . Note that the difference between the clumping factors obtained from *r[z<sub>r</sub>]L6N256* and *r19.5L6N256* becomes smaller with increasing reheating redshift  $z_r$ . In particular, the clumping factors obtained for reheating at  $z_r = 15$  are nearly identical to those obtained for reheating at  $z_r = 19.5$  at all redshifts. The evolution of the clumping factors obtained from *r19.5L6N256* can therefore be considered to reflect the evolution of the clumping factor in the limit of reheating at very high redshift,  $z_r \gg 19.5$ .

In Appendix A we provide fits to the evolution of the clumping factor over the redshift range  $6 \leq z \leq 20$  for a range of (over-)density thresholds and reheating redshifts. These fits (Eqs. A1 and A2) may be employed in (semi-)analytic models of the epoch of reionisation. Many such models assume that reionisation heating provides only a negative feedback on the reionisation process, reducing the star formation rate due to the photo-evaporation of gas in low-mass halos. However, as we have shown here, photo-heating decreases the clumping factor, and hence the average recombination rate. Since this makes it easier to keep the IGM ionised, reionisation heating also provides a positive feedback on the process of reionisation. Although the relative importance of both can only be assessed using larger hydrodynamical simulations of higher resolution<sup>6</sup>, it is clear that models that do not account for this positive feedback will underestimate the efficiency with which star-forming galaxies are able to reionise the IGM.

### 3.2.3 Dependence on the reheating temperature

In this section we investigate the robustness of our results with respect to our simplified treatment of photo-ionisation heating.

We have considered photo-heating by a uniform ionising background in the optically thin limit. In reality, the reionisation process is likely to be driven by inhomogeneously distributed sources in an initially optically thick medium. The temperature to which the IGM is reheated will then not only depend on the spectrum of the ionising sources,

<sup>6</sup> At  $z = 6$ , the cosmic SFR density (the stellar mass) in *r9L6N256* is smaller than that in *L6N256* by a factor 1.26 (1.17). In our simulations, photo-heating thus decreases the SFR density less strongly than it reduces the clumping factor, which would imply that the positive feedback is more important. The SFR densities in both *r9L6N256* and *L6N256* are, however, not fully converged with respect to resolution and box size. A final assessment as to whether the negative or the positive feedback is stronger must therefore be deferred to future studies using simulations with higher resolution and larger box sizes.

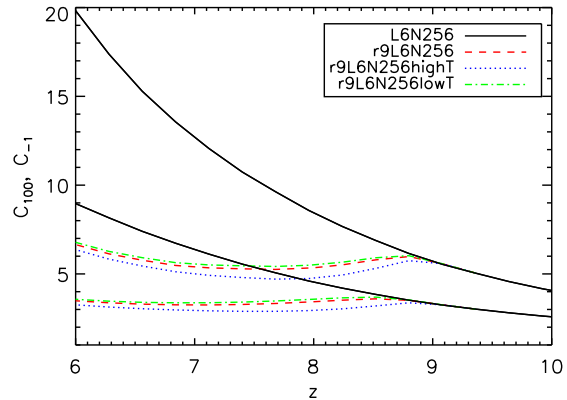


**Figure 6.** The dependence of  $C_{-1}$  (upper set of curves) and  $C_{100}$  (lower set of curves) on the value for the reheating energy  $\epsilon_r$ . Both *r9L6N256highT* ( $\epsilon_r = 20$  eV) and *r9L6N256lowT* ( $\epsilon_r = 0$  eV) give results very similar to that obtained from the default run, *r9L6N256* ( $\epsilon_r = 2$  eV), which demonstrates the robustness of our conclusions with respect to changes in the reheating temperature.

but also on the amount of spectral hardening due to the preferential absorption of the less energetic ionising photons (e.g. Abel & Haehnelt 1999; Bolton, Meiksin, & White 2004). Moreover, the speed at which a particular patch of the IGM is reionised determines the duration during which its gas can cool efficiently, as the cooling is dominated by inelastic collisions between free electrons and neutral atoms. Different reionisation histories may therefore result in different IGM temperatures (e.g. Miralda-Escudé & Rees 1994; Theuns et al. 2002; Hui & Haiman 2003; Tittley & Meiksin 2007).

To bracket possible scenarios, we have performed two additional simulations in which we varied the amount of energy transferred to the baryons during the photo-ionisation process, *r9L6N256highT* and *r9L6N256lowT*. Whereas in the former we employ an additional energy input that is ten times larger than our default value ( $\epsilon_r = 20$  eV), in the latter no additional energy is injected ( $\epsilon_r = 0$  eV). We show in Fig. 6 that the evolution of  $C_{-1}$  and  $C_{100}$  obtained from these two simulations is very similar to that obtained from our default run, *r9L6N256*. The dependence on the reheating temperature  $T_r > 10^4$  K is weak, because halos with virial temperatures  $T_{\text{vir}} \lesssim 10^4$  K are already efficiently destroyed for  $T_r \approx 10^4$  K. A further increase in the reheating temperature mostly affects the fraction of mass in halos with larger virial temperatures, which is small. Moreover, Fig. 1 shows that the gas in the simulations *r9L6N256highT* and *r9L6N256lowT* quickly loses memory of its thermal state at some higher redshift, which is another reason for the similarity in the results obtained using different values for the reheating energy  $\epsilon_r$ .

### 3.2.4 Effect of kinetic supernova feedback and dependence on cosmological parameters

The inclusion of kinetic feedback from supernovae in *r9L6N256winds* only weakly affects the evolution of the clumping factors. At redshift  $z = 6$ ,  $C_{-1}$  and  $C_{100}$

are slightly larger (by factors 1.1 and 1.18, resp.) in *r9L6N256winds* than in our default simulation, *r9L6N256*, which does not include kinetic feedback. The reason for the slight increase in the clumping factors is that winds move gas from regions of densities larger than the critical density for the onset of star formation to regions of lower density that contribute to the calculation of the clumping factors. We note that the inclusion of kinetic feedback does, on the other hand, strongly affect the cosmic SFR. At  $z = 6$ , the cosmic SFR (the stellar mass) is lower in the simulation that includes kinetic feedback (*r9L6N256winds*) than in our default simulation (*r9L6N256*) by a factor of 6.1 (3.4).

Finally, we quote the clumping factors obtained from the simulations *r9L6N256W3* and *r9L6N256W1*, which employed cosmological parameters consistent with the WMAP 3-year and 1-year observations, respectively. We find that at redshift  $z = 6$ , the clumping factors  $C_{-1}$  and  $C_{100}$  are larger in *r9L6N256* than in *r9L6N256W3* by factors of 1.31 and 1.16, respectively. They are smaller in *r9L6N256* than in *r9L6N256W1* by factors of 0.74 and 0.84. In summary, with respect to *r9L6N256*, the clumping factors are larger in *r9L6N256W1* and smaller in *r9L6N256W3*, as expected from the corresponding values of  $\sigma_8$ , which set the average absolute amplitude of the overdensity fluctuations.

## 4 DISCUSSION

Several observational studies have claimed that the star formation rate (SFR) density at redshift  $z \approx 6$  is smaller than the critical SFR density required to keep the intergalactic medium (IGM) ionised. In the absence of a large population of unseen sources of ionising radiation, this discrepancy between the two SFR densities would be in direct conflict with the high degree of ionisation inferred from the non-detection of a Gunn-Peterson trough in the majority of the line-of-sight spectra towards  $z \lesssim 6$  quasars.

The critical SFR density is inversely proportional to the fraction of ionising photons escaping into the IGM and proportional to the clumping factor  $C \equiv \langle \rho_b^2 \rangle_{\text{IGM}} / \langle \rho_b \rangle^2$ , a measure for the average recombination rate in the IGM. One may therefore ask whether the discrepancy between the observed and critical SFR densities could be resolved by changing the assumptions about the values of either of these two quantities. In this work we have considered the hypothesis that most observational studies overestimate the critical SFR density because they employ a clumping factor that is too large.

Photo-ionisation heating expels the gas from within halos of virial temperatures  $T_{\text{vir}} \lesssim 10^4$  K and prevents its further accretion by raising the Jeans mass in the IGM. By suppressing the formation of stars in these low-mass halos, photo-heating from reionisation decreases the rate at which ionising photons are emitted into the IGM and is therefore correctly said to exert a negative feedback on the reionisation process. The fact that photo-heating also leads to a decrease in the clumping factor and hence provides a strong positive feedback by making it easier to keep the IGM ionised, is however often overlooked (but see, e.g., Haiman, Abel, & Madau 2001; Oh & Haiman 2003; Kuhlen & Madau 2005; Wise & Abel 2005; Ciardi & Salvaterra 2007).

To illustrate the effect of photo-heating on the evolution of the clumping factor we have analysed the gas density distributions in a set of cosmological smoothed particle hydrodynamics simulations that include radiative cooling and photo-ionisation by a uniform UV background in the optically thin limit. The clumping factor of the IGM depends critically on the definition of which gas is considered to be part of the IGM. We assumed that all gas with densities below a threshold density constitutes the IGM and computed the clumping factor as a function of this threshold density. In addition, we introduced two physically well-motivated definitions,  $C_{100}$ , the clumping factor of gas with overdensities  $\Delta < 100$  and  $C_{-1}$ , the clumping factor of gas with densities below  $n_{\text{H}} = n_{\text{H}}^* \equiv 10^{-1} \text{ cm}^{-3}$ , our threshold density for the onset of star formation.

By comparing simulations that include photo-ionisation by a uniform UV background to one that does not, we showed that photo-heating strongly influences the evolution of the clumping factor of the IGM. At redshift  $z = 6$ , we find that  $C_{-1} \approx 6$  and  $C_{100} \approx 3$ , independent of the redshift  $z_{\text{r}}$  at which the UV background is turned on, as long as  $z_{\text{r}} \gtrsim 9$ . These values for  $C_{-1}$  and  $C_{100}$  are at least three times smaller than they would be in the absence of photo-heating. We demonstrated that our default simulation is converged at  $z = 6$  with respect to the employed simulation box size and resolution. Finally, in Appendix A we provide fits to the evolution of the clumping factor for various (over-)density thresholds and reheating redshifts for use with (semi-)analytic models of the epoch of reionisation.

Since even our most conservative estimate for the clumping factor ( $C_{-1} \approx 6$ ) is five times smaller than the clumping factor that is usually employed to determine the capacity of star-forming galaxies to keep the  $z = 6$  IGM ionised, our results may have important implications for the understanding of the reionisation process. Setting  $C = 6$  in Eq. 1, the critical SFR density becomes  $\dot{\rho}_* = 0.005 f_{\text{esc}}^{-1} \text{ M}_{\odot} \text{ yr}^{-1} \text{ Mpc}^{-3}$ . This is smaller than recent observational estimates for the SFR density at  $z \approx 6$ ,  $\dot{\rho}_* = 0.022 \pm 0.004 \text{ M}_{\odot} \text{ yr}^{-1} \text{ Mpc}^{-3}$  (integrated to the observed  $z \approx 6$  faint-end limit  $L > 0.04 L_{z=3}^*$  and dust-corrected; Bouwens et al. 2007), provided that  $f_{\text{esc}} > 0.2$ . Our study thus suggests that the observed population of star-forming galaxies may be capable of keeping the IGM ionised, relaxing the tension between observationally inferred and critical SFR density in view of the observation of a highly ionised IGM at redshifts  $z \lesssim 6$ . We note that at  $z \approx 7$ , the SFR density is estimated to be  $\dot{\rho}_* = 0.004 \pm 0.002 \text{ M}_{\odot} \text{ yr}^{-1} \text{ Mpc}^{-3}$  (integrated to the observed  $z \approx 7$  faint-end limit  $L > 0.2 L_{z=3}^*$  and dust-corrected; Bouwens et al. 2008), whereas the critical SFR density is  $\dot{\rho}_* = 0.008 f_{\text{esc}}^{-1} \text{ M}_{\odot} \text{ yr}^{-1} \text{ Mpc}^{-3}$  (using  $C = 6$ ). The observed population of star-forming galaxies at  $z \approx 7$  is therefore not able to keep the IGM ionised. If the Universe was ionised by this redshift, then the sources that were responsible remain to be discovered.

Our simulations strikingly demonstrate that radiation-hydrodynamical feedback due to photo-ionisation heating plays a key role in shaping the properties of the IGM at redshifts  $z \gtrsim 6$ . In this work, we have studied the impact of photo-ionisation heating on the clumping factor of the IGM assuming a uniform ionising UV background in the optically thin limit. In reality the reionisation process will, however, be more complex. We have demonstrated the robustness of

our conclusions with respect to uncertainties in the temperature of the IGM resulting from our simplified treatment of the reionisation heating, but there are other factors whose importance is more difficult to assess.

Low-mass halos could keep some of their gas in the presence of photo-ionisation heating due to self-shielding. The self-shielded gas in these halos is neutral and hence does not contribute to the average recombination rate of the IGM. This gas should therefore be excluded when computing the clumping factor. Self-shielding becomes important for  $N_{\text{HI}} \gtrsim 10^{18} \text{ cm}^{-2}$ , which for self-gravitating gas clouds corresponds to densities (Schaye 2001)  $n_{\text{H}} \gtrsim 10^{-2} \text{ cm}^{-3} (\Gamma/10^{-12} \text{ s}^{-1})^{-1}$ , where  $\Gamma$  is the HI photo-ionization rate. Our use of  $C_{-1}$  therefore results in a very conservative estimate of the clumping factor of the IGM. Miralda-Escudé, Haehnelt, & Rees (2000) discussed the validity of the assumption of a uniform ionised fraction, implicit to our analysis, and found that it does not significantly affect the calculation of the clumping factor. On the other hand, Furlanetto, Haiman, & Oh (2008) point out that because denser gas recombines faster, it is the gas of lowest density that determines the value for the clumping factor for large parts of the time. Since the clumping factor associated with gas of lower densities is smaller, this would, however, only strengthen our conclusions. Another simplifying assumption underlying our analysis is that of the primordial chemical composition of the gas in our simulations. The presence of metals and molecules will increase the ability of the gas to cool and hence may slightly increase the clumping factor (e.g. Maio et al. 2007). However, in the presence of photo-heating and for the threshold densities we employ we expect this effect to be very small. A more precise assessment of the clumping factor that takes care of these and other issues can, however, only be obtained using full radiation-hydrodynamical simulations including cooling by metals and molecules.

We have recently developed a radiative transfer scheme (TRAPHIC; Pawlik & Schaye 2008) that allows us to study the time-dependent radiative transfer problem self-consistently in spatially adaptive SPH simulations containing a large number of ionising sources. We will report on detailed radiation-hydrodynamical simulations employing TRAPHIC to study the hydrodynamical response of gas to radiation heating from a non-uniform UV radiation field and its implications for the clumping factor of the IGM in future work.

## ACKNOWLEDGMENTS

We thank Rychard Bouwens for a valuable discussion on the observed star formation rates. We are grateful to Claudio Dalla Vecchia for help with running the simulations, Rob Wiersma for useful discussions on the cooling tables and Marcel Haas and Freeke van der Voort for a thorough reading of the draft. The simulations presented here were run on the Cosmology Machine at the Institute for Computational Cosmology in Durham as part of the Virgo Consortium research programme and on Stella, the LOFAR BlueGene/L system in Groningen. This work was supported by Marie Curie Excellence Grant MEXT-CT-2004-014112.

## REFERENCES

- Abel T., Haehnelt M. G., 1999, *ApJ*, 520, L13  
 Barkana R., Loeb A., 1999, *ApJ*, 523, 54  
 Barkana R., Loeb A., 2001, *PhR*, 349, 125  
 Benson A. J., Nusser A., Sugiyama N., Lacey C. G., 2001, *MNRAS*, 320, 153  
 Bolton J., Meiksin A., White M., 2004, *MNRAS*, 348, L43  
 Bolton J. S., Haehnelt M. G., 2007, *MNRAS*, 382, 325  
 Bouwens R. J., et al., 2004, *ApJ*, 606, L25  
 Bouwens R. J., Illingworth G. D., Blakeslee J. P., Franx M., 2006, *ApJ*, 653, 53  
 Bouwens R. J., Illingworth G. D., Franx M., Ford H., 2007, *ApJ*, 670, 928  
 Bouwens R. J., Illingworth G. D., Franx M., Ford H., 2008, preprint (arXiv:0803.0548)  
 Bruzual G., Charlot S., 2003, *MNRAS*, 344, 1000  
 Bunker A. J., Stanway E. R., Ellis R. S., McMahon R. G., 2004, *MNRAS*, 355, 374  
 Chabrier G., 2003, *PASP*, 115, 763  
 Chiu W. A., Fan X., Ostriker J. P., 2003, *ApJ*, 599, 759  
 Ciardi B., Salvaterra R., 2007, *MNRAS*, 381, 1137  
 Collin-Souffrin S., 1991, *A&A*, 243, 5  
 Chuzhoy L., Kuhlen M., Shapiro P. R., 2007, *ApJ*, 665, L85  
 Dalla Vecchia C., Schaye J., 2008, *MNRAS*, 387, 1431  
 Dijkstra M., Haiman Z., Rees M. J., Weinberg D. H., 2004, *ApJ*, 601, 666  
 Efstathiou G., 1992, *MNRAS*, 256, 43P  
 Fan X., Carilli C. L., Keating B., 2006, *ARA&A*, 44, 415  
 Ferland G. J., Korista K. T., Verner D. A., Ferguson J. W., Kingdon J. B., Verner E. M., 1998, *PASP*, 110, 761  
 Furlanetto S. R., Oh S. P., Briggs F. H., 2006, *PhR*, 433, 181  
 Furlanetto S., Haiman Z., Oh S. P., 2008, preprint (arXiv:0803.3454)  
 Glover S. C. O., Brand P. W. J. L., 2003, *MNRAS*, 340, 210  
 Glover S. C. O., 2007, *MNRAS*, 379, 1352  
 Gnedin N. Y., Ostriker J. P., 1997, *ApJ*, 486, 581  
 Gnedin N. Y., Hui L., 1998, *MNRAS*, 296, 44  
 Gnedin N. Y., 2000a, *ApJ*, 535, 530  
 Gnedin N. Y., 2000b, *ApJ*, 542, 535  
 Gnedin N. Y., Kravtsov A. V., Chen H.-W., 2008, *ApJ*, 672, 765  
 Haardt F., Madau P., 2001, in the proceedings of XXXVI Rencontres de Moriond, preprint (astro-ph/0106018)  
 Haiman Z., Rees M. J., Loeb A., 1997, *ApJ*, 476, 458  
 Haiman Z., Abel T., Madau P., 2001, *ApJ*, 551, 599  
 Hui L., Haiman Z., 2003, *ApJ*, 596, 9  
 Iliev I. T., Mellema G., Shapiro P. R., Pen U.-L., 2007, *MNRAS*, 376, 534  
 Inoue A. K., Iwata I., Deharveng J.-M., 2006, *MNRAS*, 371, L1  
 Kennicutt R. C., Jr., 1998, *ApJ*, 498, 541  
 Kitayama T., Ikeuchi S., 2000, *ApJ*, 529, 615  
 Kohler K., Gnedin N. Y., Hamilton A. J. S., 2007, *ApJ*, 657, 15  
 Komatsu E., et al., 2008, preprint (arXiv:0803.0547)  
 Kuhlen M., Madau P., 2005, *MNRAS*, 363, 1069  
 Lacey C., Cole S., 1994, *MNRAS*, 271, 676  
 Machacek M. E., Bryan G. L., Abel T., 2003, *MNRAS*, 338, 273

Madau P., Efstathiou G., 1999, ApJ, 517, L9  
 Madau P., Haardt F., Rees M. J., 1999, ApJ, 514, 648  
 Madau P., 2000, RSPTA, 358, 2021  
 Madau P., Rees M. J., Volonteri M., Haardt F., Oh S. P., 2004, ApJ, 604, 484  
 Maio U., Dolag K., Ciardi B., Tornatore L., 2007, MNRAS, 379, 963  
 Mannucci F., Buttery H., Maiolino R., Marconi A., Pozzetti L., 2007, A&A, 461, 423  
 Mesinger A., Dijkstra M., 2008, preprint (arXiv:0806.3090)  
 Miralda-Escudé J., Rees M. J., 1994, MNRAS, 266, 343  
 Miralda-Escudé J., Haehnelt M., Rees M. J., 2000, ApJ, 530, 1  
 Miralda-Escudé J., 2003, ApJ, 597, 66  
 Navarro J. F., Steinmetz M., 1997, ApJ, 478, 13  
 Oesch P. A., et al., 2008, preprint (arXiv:0804.4874)  
 Oh S. P., 2001, ApJ, 553, 499  
 Oh S. P., Haiman Z., 2003, MNRAS, 346, 456  
 Okamoto T., Gao L., Theuns T., 2008, preprint (arXiv:0806.0378)  
 Padmanabhan T., Structure Formation in the Universe, Cambridge University Press (1993)  
 Pawlik A. H., Schaye J., 2008, MNRAS, accepted, preprint (arXiv:0802.1715)  
 Razoumov A. O., Sommer-Larsen J., 2006, ApJ, 651, L89  
 Ricotti M., Ostriker J. P., 2004, MNRAS, 352, 547  
 Sawicki M., Thompson D., 2006, ApJ, 648, 299  
 Schaye J., 2001, ApJ, 559, 507  
 Schaye J., 2004, ApJ, 609, 667  
 Schaye J., Dalla Vecchia C., 2008, MNRAS, 383, 1210  
 Seljak U., Zaldarriaga M., 1996, ApJ, 469, 437  
 Shapiro P. R., Giroux M. L., Babul A., 1994, ApJ, 427, 25  
 Shapiro P. R., Iliev I. T., Raga A. C., 2004, MNRAS, 348, 753  
 Shapley A. E., Steidel C. C., Pettini M., Adelberger K. L., 2003, ApJ, 588, 65  
 Spergel D. N., et al., 2007, ApJS, 170, 377  
 Spergel D. N., et al., 2003, ApJS, 148, 175  
 Springel V., Hernquist L., 2003, MNRAS, 339, 289  
 Springel V., 2005, MNRAS, 364, 1105  
 Srbnovsky J. A., Wyithe J. S. B., 2007, MNRAS, 374, 627  
 Stanway E. R., Bunker A. J., McMahon R. G., 2003, MNRAS, 342, 439  
 Stiavelli M., Fall S. M., Panagia N., 2004, ApJ, 610, L1  
 Theuns T., Schaye J., Zaroubi S., Kim T.-S., Tzanavaris P., Carswell B., 2002, ApJ, 567, L103  
 Thoul A. A., Weinberg D. H., 1996, ApJ, 465, 608  
 Tittley E. R., Meiksin A., 2007, MNRAS, 380, 1369  
 Valageas P., Silk J., 1999, A&A, 347, 1  
 Veilleux S., Cecil G., Bland-Hawthorn J., 2005, ARA&A, 43, 769  
 Venkatesan A., Giroux M. L., Shull J. M., 2001, ApJ, 563, 1  
 Wiersma R. P. C., Schaye J., Smith B. D., 2008, MNRAS, submitted, preprint (arXiv:0807.3748)  
 Wise J. H., Abel T., 2005, ApJ, 629, 615

$6 \leq z \leq 20$ , based on the data presented in Fig. 5. In addition, we give fits to the evolution of the clumping factors  $C_{-2}$  and  $C_{1000}, C_{500}, C_{200}$  and  $C_{50}$ , where  $C_{-2} \equiv C(< 10^{-2} \text{ cm}^{-3} m_{\text{H}} / (X \langle \rho_{\text{b}} \rangle))$  and  $C_{1000} \equiv C(< \min(1000, 10^{-1} \text{ cm}^{-3} m_{\text{H}} / (X \langle \rho_{\text{b}} \rangle)))$  and similar for  $C_{500}, C_{200}$  and  $C_{50}$ . We first give fits to the evolution of the clumping factors for the simulations *L6N256* and *r19.5L6N256*, i.e. the simulations without reheating and with reheating at the highest redshift we considered. These fits are then used to obtain fits to the evolution of the clumping factors for reheating at the intermediate redshifts  $z_r = 7.5, 9.0, 10.5, 12, 13.5$  and  $15.0$  by interpolation.

We approximate the evolution of the clumping factors for the simulations *L6N256* and *r19.5L6N256* by

$$C(z) = z^{\beta} e^{-\gamma z + \delta} + \alpha, \quad (\text{A1})$$

where  $C$  is either  $C_{-1}, C_{-2}, C_{1000}, C_{500}, C_{200}, C_{100}$  or  $C_{50}$  and similar for  $\alpha, \beta, \gamma, \delta$ . The values for the parameters  $\alpha, \beta, \gamma, \delta$  are listed in Tables A1 and A2. The fit (Eq. A1) is accurate to within  $\lesssim 10\%$ . We emphasize that it is only strictly valid over the fitting range  $6 \leq z \leq 20$ . For  $C_{1000}, C_{500}, C_{200}, C_{100}$  and  $C_{50}$ , i.e. for the clumping factors that are defined using an overdensity threshold, we forced, however, the fits to approach the correct high- $z$  limit, i.e.  $C \rightarrow 1$ , by fixing  $\alpha = 1$  during the fitting procedure. Note that the threshold densities used with  $C_{-1}$  and  $C_{-2}$  correspond to negative threshold overdensities for redshifts  $z > 79.4$  and  $z > 36.3$ , respectively and that  $C_{1000}, C_{500}, C_{200}, C_{100}$  and  $C_{50}$  become identical to  $C_{-1}$  for redshifts  $z > 7.0, 9.1, 12.7, 16.3$  and  $20.8$ , respectively.

The values of  $C$  for reheating at redshifts  $z_r = 7.5, 9.0, 10.5, 12, 13.5$  and  $15.0$  (hereafter  $C^{z_r}$ ) are obtained by interpolating between the fits (Eq. A1) to the evolution of the clumping factors obtained from *L6N256* (hereafter  $C^0$ ) and *r19.5L6N256* (hereafter  $C^{19.5}$ ). We write

$$C^{z_r}(z) = w(z)C^0(z) + [1 - w(z)]C^{19.5}(z), \quad (\text{A2})$$

where

$$w(z) = \frac{1}{2} \left[ \text{erf} \left( \frac{z - \zeta^{z_r}}{\tau^{z_r}} \right) + 1 \right], \quad (\text{A3})$$

and erf is the error function,

$$\text{erf}(z) = \frac{2}{\sqrt{\pi}} \int_0^z d\tilde{z} \exp(-\tilde{z}^2). \quad (\text{A4})$$

The constants  $\zeta^{z_r}$  and  $\tau^{z_r}$  are listed in Tables A3 and A4. Eq. A2 fits the data to within  $\lesssim 10\%$ .

This paper has been typeset from a  $\text{T}_{\text{E}}\text{X}/\text{L}^{\text{A}}\text{T}_{\text{E}}\text{X}$  file prepared by the author.

## APPENDIX A: FITTING FORMULAS

In this appendix we provide fits to the evolution of the clumping factors  $C_{-1}$  and  $C_{100}$  over the redshift range

**Table A4.** Parameter values  $\zeta^{z_r}$  and  $\tau^{z_r}$  to be used in Eq. A2 in order to fit the evolution of the clumping factors  $C_{1000}, C_{500}, C_{200}, C_{100}$  and  $C_{50}$  obtained from the simulations  $r[z_r]L6N256$  (see also Fig. 5).

$z_r$	$\zeta_{1000}^{z_r}$	$\tau_{1000}^{z_r}$	$\zeta_{500}^{z_r}$	$\tau_{500}^{z_r}$	$\zeta_{200}^{z_r}$	$\tau_{200}^{z_r}$	$\zeta_{100}^{z_r}$	$\tau_{100}^{z_r}$	$\zeta_{50}^{z_r}$	$\tau_{50}^{z_r}$
7.5	6.71	0.68	6.74	0.76	6.71	0.83	6.60	0.75	6.53	0.85
9.0	7.98	1.29	7.96	1.22	7.93	1.32	7.75	1.72	7.67	1.37
10.5	9.49	2.00	9.50	2.12	9.33	2.03	8.99	1.71	8.94	2.03
12.0	11.10	2.58	11.33	3.05	10.98	2.90	10.39	2.38	10.40	2.84
13.5	12.36	2.35	13.12	3.63	12.75	3.72	11.93	3.07	12.02	3.69
15.0	13.27	1.77	14.36	3.26	14.64	4.49	13.66	3.75	13.86	4.60

**Table A1.** Parameter values  $\alpha, \beta, \gamma$  and  $\delta$  to be used in Eq. A1 in order to fit the evolution of the clumping factors  $C_{-1}$  and  $C_{-2}$  obtained from the simulations  $L6N256$  and  $r19.5L6N256$  (see also Fig. 5).

	$L6N256$	$r19.5L6N256$
$\alpha_{-1}$	1.29	1.21
$\beta_{-1}$	0.00	-3.66
$\gamma_{-1}$	0.47	0.00
$\delta_{-1}$	5.76	8.25
$\alpha_{-2}$	1.29	1.16
$\beta_{-2}$	0.00	-2.47
$\gamma_{-2}$	0.44	0.00
$\delta_{-2}$	4.68	5.16

**Table A3.** Parameter values  $\zeta^{z_r}$  and  $\tau^{z_r}$  to be used in Eq. A2 in order to fit the evolution of the clumping factors  $C_{-1}$  and  $C_{-2}$  obtained from the simulations  $r[z_r]L6N256$  (see also Fig. 5).

$z_r$	$\zeta_{-1}^{z_r}$	$\tau_{-1}^{z_r}$	$\zeta_{-2}^{z_r}$	$\tau_{-2}^{z_r}$
7.5	6.83	0.83	6.61	0.80
9.0	8.10	1.25	7.78	1.26
10.5	9.41	1.71	8.92	1.65
12.0	10.77	2.16	10.02	1.96
13.5	12.10	2.45	11.09	2.24
15.0	13.27	2.43	12.20	2.48

**Table A2.** Parameter values  $\alpha, \beta, \gamma$  and  $\delta$  to be used in Eq. A1 in order to fit the evolution of the clumping factors  $C_{1000}, C_{500}, C_{200}, C_{100}$  and  $C_{50}$  obtained from the simulations  $L6N256$  and  $r19.5L6N256$  (see also Fig. 5).

	$L6N256$	$r19.5L6N256$
$\alpha_{1000}$	1.00	1.00
$\beta_{1000}$	-1.00	-2.89
$\gamma_{1000}$	0.28	0.00
$\delta_{1000}$	6.29	6.76
$\alpha_{500}$	1.00	1.00
$\beta_{500}$	0.00	-2.44
$\gamma_{500}$	0.34	0.00
$\delta_{500}$	4.60	5.68
$\alpha_{200}$	1.00	1.00
$\beta_{200}$	0.00	-1.99
$\gamma_{200}$	0.30	0.00
$\delta_{200}$	4.04	4.49
$\alpha_{100}$	1.00	1.00
$\beta_{100}$	0.00	-1.71
$\gamma_{100}$	0.28	0.00
$\delta_{100}$	3.59	3.76
$\alpha_{50}$	1.00	1.00
$\beta_{50}$	0.00	-1.47
$\gamma_{50}$	0.23	0.00
$\delta_{50}$	2.92	3.08